GSC Biological and Pharmaceutical Sciences
eISSN: 2581-3250 CODEN (USA): GBPSC2
Cross Ref DOI: 10.30574/gscbps
Journal homepage: https://gsconlinepress.com/journals/gscbps/

(RESEARCH ARTICLE)

Check for updates

Investigation of the biological activities of a polyethyleneimine-Schiff base functionalized nitrogen-doped graphene quantum dot and silver nanocomposite

Elif Ünaldı [1] and Neslihan Güleç [2,*]

[1] *Department of Biology, Çanakkale Onsekiz Mart University, School of Graduate Studies, 17100 Çanakkale, Türkiye.*
[2] *Department of Biology, Faculty of Science, Çanakkale Onsekiz Mart University, 17100 Çanakkale, Türkiye.*

GSC Biological and Pharmaceutical Sciences, 2025, 33(03), 068-081

Publication history: Received 28 October 2025; revised on 02 December 2025; accepted on 05 December 2025

Article DOI: https://doi.org/10.30574/gscbps.2025.33.3.0483

Abstract

The biological activities of original 5-methylsalicylaldehyde-polyethyleneimine Schiff base functionalized nitrogen-doped graphene quantum dot (5-MESAL-PEI N-GQD) and its silver nanocomposite (AgNP/5-MESAL-PEI N-GQD) were investigated. 5-MESAL-PEI N-GQD and AgNP/5-MESAL-PEI N-GQD were characterized using Fourier Transform Infrared Spectroscopy (FT-IR), Scanning Electron Microscopy (SEM), Energy Dispersive X-ray Spectroscopy (EDS), and Transmission Electron Microscopy (TEM). DNA-binding interactions were evaluated using Calf Thymus - Deoxyribonucleic Acid (CT-DNA) via UV-Vis absorption spectroscopy, while DNA cleavage activity was analyzed by agarose gel electrophoresis using pBR322 plasmid DNA. The antimicrobial activity was assessed by determining the minimum inhibitory concentration (MIC) against various bacterial and yeast strains. Antibiofilm activity was evaluated through the microplate assay using different microbial strains. Antioxidant properties were investigated by 1,1-diphenyl-2picryhydrazyl (DPPH) radical scavenging activity, 2,2′-Azino-bis(3-ethylbenzothiazoline-6-sulfonic acid) (ABTS) cation radical scavenging assay, and ferric reducing antioxidant power (FRAP) assay. As a result, both 5-MESAL-PEI N-GQD and AgNP/5-MESAL-PEI N-GQD exhibited electrostatic interactions with CT-DNA and were found to induce both hydrolytic and oxidative cleavage of supercoiled pBR322 plasmid DNA in a concentration-dependent manner. AgNP/5-MESAL-PEI N-GQD was demonstrated higher antimicrobial activity compared to 5-MESAL-PEI N-GQD. Furthermore, both compounds exhibited strong antibiofilm effects against the tested microbial strains. As a conclusion, the antibacterial, antibiofilm, antioxidant, and DNA interaction properties of these nanomaterials suggest that they could serve as promising bioactive agents for both biotechnological and clinical applications.

Keywords: Nitrogen-Doped Graphene Quantum Dots; Silver Nanocomposite; DNA Binding; DNA Cleavage; Antimicrobial Activity; Antioxidant Properties

1. Introduction

Graphene is a two-dimensional nanomaterial consisting of carbon atoms arranged in a hexagonal lattice, characterized by its exceptionally high surface area, thermal stability, remarkable electrical conductivity, optical transparency, and mechanical flexibility [1, 2]. Owing to these versatile characteristics, graphene has attracted significant attention in various fields, including nanoelectronics, biomedicine, energy storage, and composite material production. Sharing its elemental composition with graphite-which has long been used due to its non-toxic nature-graphene has also been regarded as a safe material for biomedical applications [3, 4]. In recent years, graphene-based materials have been widely studied for applications such as photocatalysis [5], heavy metal ion removal [6], drug delivery systems [7], and degradation of organic pollutants [8]. In this context, the development of graphene-polymer nanocomposites has become an area of growing research interest [9].

* Corresponding author: Neslihan Güleç

Graphene quantum dots (GQDs), owing to their high biocompatability, favorable optical properties, and readily functionalizable surfaces, are utilized in a broad range of applications, including biosensing, imaging, drug delivery, and antibacterial coatings. Their nitrogen-doped derivatives exhibit superior features such as an improved electronic structure, enhanced electron transfer, and stronger interactions with biological systems. Notably, the ability of positively charged N-GQDs to form stable electrostatic complexes with negatively charged genetic materials, combined with their biocompatible and degradable nature, highlights their potential as promising non-viral gene-delivery platforms [10].

Silver nanoparticles (AgNPs) are metallic nanostructures known for their antimicrobial and anticancer activities, and they are widely used in various fields such as medicine, textiles, sensor technologies, and catalysis [11, 12]. Their low cost and strong interaction capability with biological systems encourage further research on these nanostructures [13].

To enhance the effectiveness of nanomaterials in biological systems, nitrogen-doped graphene quantum dots (N-GQDs) were modified with polyethyleneimine (PEI) through Schiff base functionalization. These nanostructures were first reported in the literature by Hançe et al. [14]. Experimental and theoretical characterizations revealed that these structures hold promising potential for theranostic applications, combining both diagnostic and therapeutic functions.

GQDs are nanostructures capable of interacting non-covalently with DNA due to the functional groups on their surfaces. These interactions typically occur through electrostatic forces between the negatively charged phosphate backbone of DNA and the positively charged or hydrophilic functional groups present on the surface of the GQDs [15]. Non-covalent interactions are crucial in biosystems due to their reversibility and specificity, playing essential roles in molecular recognition and transport processes. Such interactions can be detected by UV-Vis spectroscopy through hyperchromism (increased absorbance) and bathochromic shift (red shifts in wavelength) [16]. These findings support the potential of GQDs in biotechnological applications involving DNA recognition and delivery.

The increasing prevalence of antimicrobial resistance and the ability of microorganisms to form protective biofilms have intensified the need for next generation antimicrobial agents. In this regard, the antibacterial and antibiofilm properties of GQDs and carbon dots have received significant attention [17]. Notably, GQD-based materials, including wound dressings, have demonstrated synergistic antibacterial activity in the presence of low concentrations of H_2O_2, offering promising potential for wound healing applications [18].

In addition, it is well known that oxidative stress caused by reactive oxygen species (ROS) can lead to the disruption of intracellular structures and the development of various diseases [19]. Antioxidant agents play a critical role in maintaining balance within biological systems by suppressing the effects of ROS. The antioxidant capacity of GQDs demonstrated through methods such as DPPH, ABTS, and FRAP highlights their potential as bioactive agents [20-22].

In the present study, 5-MESAL-PEI Schiff base functionalized N-GQD and its Ag-doped nanocomposite (AgNP/5-MESAL-PEI N-GQD) were synthesized and comprehensively characterized for the first time. The DNA interaction mechanisms (binding and cleavage), antimicrobial, antibiofilm activities, and antioxidant capacities of these nanostructures were systematically evaluated to gain a deeper understanding of their biological functionality.

2. Material and Methods

2.1. Materials

All chemicals and reagents used in the synthesis were supplied by Sigma-Aldrich and Merck. All solutions were freshly prepared prior to the experiments, and necessary pH adjustments were carried out using appropriate buffer.

2.2. Methods

2.2.1. Synthesis of 5-MESAL-PEI N-GQD Schiff base and AgNP/5-MESAL-PEI N-GQD nanocomposite

PEI N-GQD (0.14 g), ethanol (150 mL), and 5-methylsalicylaldehyde (0.14 g) were added to a 250 mL round-bottom flask. The mixture was refluxed for 3 h. After evaporation of ethanol, the resulting yellow solid identified as 5-MESAL-PEI N-GQD, was collected, washed with hot ethanol, and dried in a vacuum oven.

In this study, 5-MESAL-PEI N-GQD (0.1304 g) was placed in a 250 mL round-bottom flask and dissolved in 100 mL of distilled water. Subsequently, 50 mL of an aqueous $AgNO_3$ solution (0.131 g) was added gradually under continuous stirring. The mixture was heated in a water bath at 90 °C for 2 hours to, resulting in the formation of the AgNP/5-MESAL-

PEI N-GQD nanocomposite. During this process, the color of the solution gradually changed from yellow to gray-black, indicating the complete reduction of Ag^+ ions to metallic silver. The final nanocomposite was washed twice with distilled water and dried in a vacuum oven.

The chemical structure of the nitrogen-doped graphene quantum dot with an imino functional group containing an electron-donating moiety, and its silver-graphene nanocomposite obtained at the end of the synthesis, is presented in Figure 1.

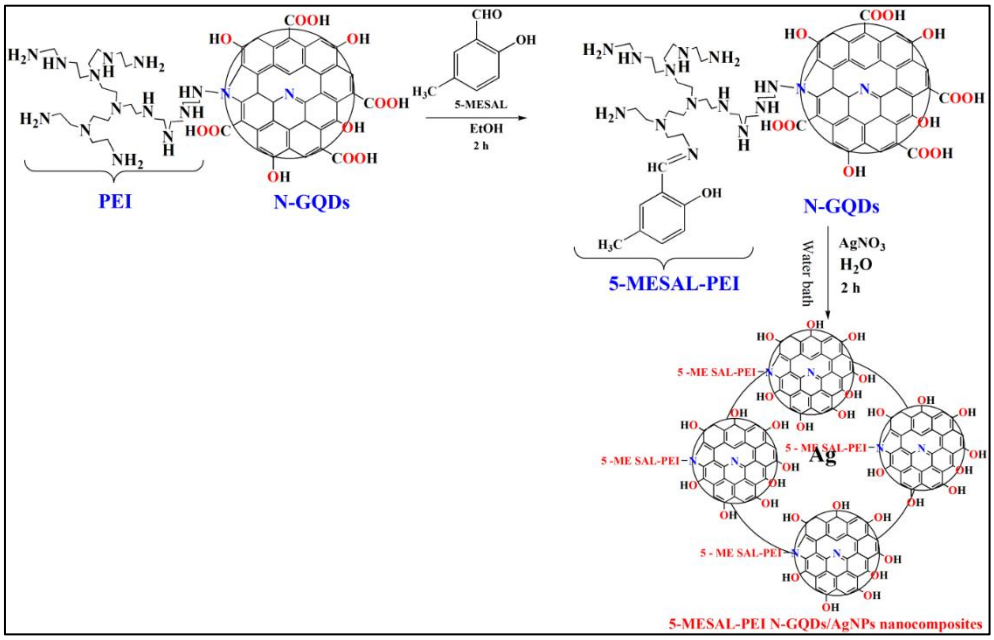

Figure 1 Synthesis of 5-MESAL-PEI N-GQD Schiff base and AgNP/5-MESAL-PEI N-GQD Schiff base nanocomposite

2.2.2. Functional, morphological, and elemental characterization of graphene quantum dots (GQDs)

Fourier Transform Infrared Spectroscopy (FT-IR) was used to determine the functional groups present on the surface of the GQDs. The surface morphology was examined using Scanning Electron Microscopy (SEM), which the presence of agglomeration were also evaluated. Internal morphology and particle size distribution were further analyzed using Transmission Electron Microscopy (TEM). Elemental composition of the GQDs was determined through Energy Dispersive X-ray Spectroscopy (EDS), allowing detailed investigation of the chemical structure.

2.2.3. Evaluation of nanomaterial-DNA interactions through UV-Vis spectroscopy

Calf Thymus DNA (CT-DNA) was used to evaluate the DNA binding ability of the synthesized compounds. UV-Vis spectrophotometric titrations were performed to monitor interactions with CT-DNA. Solutions of the compounds prepared in TNE buffer (8 mM Tris-HCl, 50 mM NaCl, and 1 mM EDTA, pH 7.4) were titrated with increasing concentrations of CT-DNA. After each addition, mixtures were incubated for 5 minutes, and absorbance was recorded from 200 to 600 nm using a T+80 UV-Vis spectrophotometer.

The percentage hypochromicity (H%) was calculated as follows:

$$H\% = \left(\frac{Ai - As}{Ai}\right) \times 100 \quad (1)$$

In the equation, Ai represents the absorbance intensity of the compound, while As corresponds to the absorbance at the highest concentration of DNA added incrementally.

2.2.4. Evaluation of DNA cleavage activity through agarose gel electrophoresis

Commercially obtained pBR322 plasmid DNA (Thermo Scientific) and six different concentrations of the compounds were used following the method described by Qiao et al. [23]. The *in vitro* DNA cleavage activities of the compounds were examined under both hydrolytic and oxidative conditions.

For the hydrolytic DNA cleavage assay, Tris-HCl buffer (10 mM, pH 7.4) was used together with pBR322 plasmid DNA and the respective compound concentrations. For the oxidative DNA cleavage assay, hydrogen peroxide (H_2O_2) was added as the oxidizing agent. The mixtures were incubated at 37 °C for approximately 3 h to allow sufficient interaction between the compounds and DNA. A 1X TAE buffer (40 mM Tris, 20 mM acetic acid, 1 mM EDTA, pH 8.2) was used for gel preparation and electrophoresis. Ethidium bromide (EtBr) was added to the gel as a fluorescent intercalating dye. After incubation, samples were mixed with 6X loading dye (30% glycerol, 0.5 M EDTA, 0.3% bromophenol blue, and 0.3% xylene cyanol) and subjected to electrophoresis at 60 V for 90 min.

2.2.5. Evaluation of antimicrobial activity based on minimum inhibitory concentration (MIC)

Antibacterial and antifungal activities were evaluated using various bacterial and yeast strains. The Gram-negative bacteria included *Proteus vulgaris* (NRRL-B-123), *Pseudomonas aeruginosa* (ATCC 27853) and *Escherichia coli* (ATCC 25922), while the Gram-positive strains included *Staphylococcus aureus* (ATCC 25923), *Bacillus subtilis* (ATCC 6633), and *Enterococcus faecalis* (ATCC 29212). Yeast strains *Candida albicans* (ATCC 10231) and *Candida tropicalis* (ATCC 1021) were used for antifungal assessment. Ampicillin and fluconazole were used as standard reference antibiotics. The antimicrobial activity of the compounds was determined using the broth microdilution method based on the guidelines provided by the Clinical and Laboratory Standards Institute [24], and minimum inhibitory concentration (MIC) values were determined [25].

2.2.6. Determination of biofilm inhibition capacity

The biofilm inhibition activity of the synthesized compounds was determined using the microplate assay method described by Merritt et al. [26]. The experiments were performed at concentrations corresponding to the MIC values of the tested compounds. Absorbance measurements were recorded at 550 nm using a microplate reader (LTEK INNO).

The percentage of biofilm inibition was calculated using the following equation:

$$\text{Biofilm Inhibition (\%)} = \left(\frac{\text{AC-AS}}{\text{AC}}\right) \times 100 \qquad (2)$$

AC: Absorbance of the control and AS: Absorbance of the sample

2.2.7. In vitro antioxidant activity assessment

The antioxidant properties of the synthesized compounds were evaluated using three common assays-DPPH, ABTS, and FRAP- chosen due to their relatively short analysis time, low cost, ease of operation, and lack of specialized equipment requirements. The antioxidant activities of all compounds were determined in a concentration-dependent manner by comparing the results obtained from the spectrophotometric procedures which are based on electron transfer reactions. All experiments were performed in triplicate.

Determination of 1,1-Diphenyl-2-picrylhydrazyl (DPPH) radical scavenging activity

The DPPH assay was performed according to the method described by Blois [27]. Stock solutions were prepared and diluted to obtain working concentrations of 12.5, 25, 50, 100, and 200 ppm. In this assay, 1000 µL of DPPH solution was mixed with 1000 µL of each compound concentration in disposable cuvettes. The mixtures were incubated in the dark at room temperature for 30 minutes. The butylated hydroxytoluene (BHT) standard and DPPH solution were used as positive and negative controls, respectively. The absorbance values were recorded at 517 nm using a UV-Vis spectrophotometer.

The radical scavenging activity was calculated using Equation 3.

$$\text{Scavenging Activity (\%)} = \left(\frac{\text{AC-AS}}{\text{AC}}\right) \times 100 \qquad (3)$$

AC: Absorbance of the control and AS: Absorbance of the sample

Determination of 2,2′-Azino-bis(3-ethylbenzothiazoline-6-sulfonic acid) (ABTS) cation radical scavenging activity

The ABTS radical scavenging activity was performed following Re et al. [28]. The ABTS reagent was prepared by mixing equal volumes of ABTS solution (7 mM) and 2.45 mM potassium persulfate (2.45 mM). This mixture was incubated in the dark at room temperature overnight to generate ABTS radicals. The resulting solution was diluted with ethanol until

its absorbance reached 0.7 at 734 nm. Compound solutions (12.5-200 ppm) were mixed with the ABTS reagent and incubated 6 min. After incubation, the absorbance values were recorded at 734 nm.

The scavenging activity was calculated using Equation 3.

Determination of ferric reducing antioxidant power (FRAP)

The FRAP assay was performed based on the method described by Benzie and Strain [29]. This method quantifies antioxidant capacity of the compounds by monitoring the formation of the Prussian blue-colored Fe^{2+}-TPTZ (2,4,6-tris(2-pyridyl)-s-triazine) complex generated through the reduction of the Fe^{3+}-TPTZ complex. Absorbance measurements were performed at 593 nm using a UV-Vis spectrophotometer. For each sample, FRAP reagent (0.3 M sodium acetate buffer, 10 mM TPTZ, and 20 mM $FeCl_3$) in a 10:1:1 ratio was added, and the mixtures were incubated in the dark for 30 minutes.

3. Results and Discussion

3.1. Characterization of 5-MESAL-PEI N-GQD Schiff Base and AgNP/5-MESAL-PEI N-GQD nanocomposites

The FT-IR spectrum exhibits broad bands and characteristic peaks indicating the presence of functional groups such as -OH, -NH, -NH_2, C=O, C=N, and C-O within the structure of the compound. These findings confirm that the compound contains aromatic and biologically active groups. In the spectrum presented in Figure 2, a comparison between 5-MESAL-PEI N-GQD and the Ag nanoparticle complex shows that certain bands shift after complexation. These shifts indicate that coordination interactions between Ag ions and the surface functional groups, confirming that complexation has occurred.

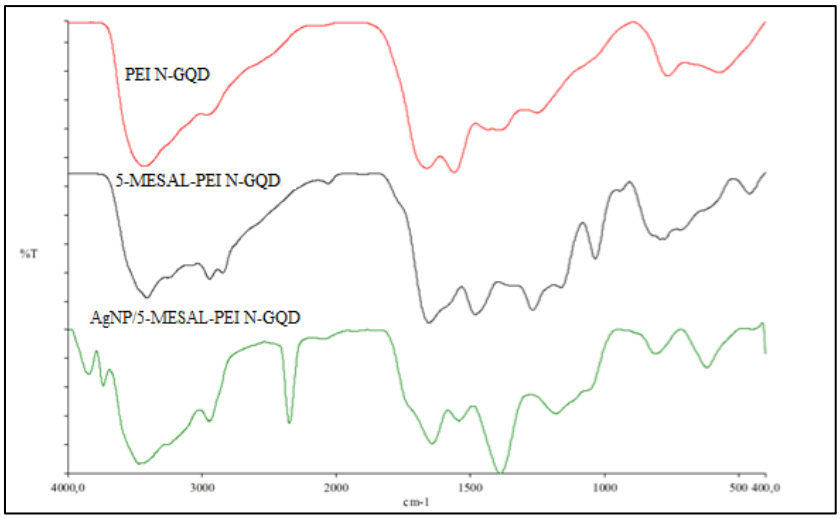

Figure 2 FT-IR spectrum of 5-MESAL-PEI N-GQD and AgNP/5-MESAL-PEI N-GQD

FT-IR (KBr, cm-1); νOH; 3472, ν [NH2+NH+COOH]; 3412-3253, νAr-H; 3078, νC-H; 2944-2841, νC=O; 1765, ν (C=Npyridinic+ C=Nimine]) 1657, νC=C; 1587, νC-N; 1485, νC-O; 1370.

The morphological properties and elemental composition of the GQDs were characterized using high-resolution imaging and analytical techniques. The surface morphologies of 5-MESAL-PEI N-GQD and AgNP/5-MESAL-PEI N-GQD were examined by SEM analysis, conducted through external service procurement. According to the SEM micrographs, the SEM image of the 5-MESAL-PEI N-GQD structures reveals a dense, closely packed morphology with a distinct granular and rod-like structure on the surface. It is observed that the particles aggregate irregularly to form compact aggregates, and the surface exhibits a distinct microtexture (Figure 3A). The SEM image of the composite structure shows that the AgNP/5-MESAL-PEI N-GQD material has a more heterogeneous, porous, and dispersed surface morphology. In this region, the particles are smaller, more irregular, and less prone to aggregation (Figure 3B). It is understood that the composite formation changes the overall structure of the surface, giving it a more amorphous appearance. When the two images are evaluated together, it is concluded that the addition of AgNP significantly affects the surface topography, heterogeneizes the distribution of the nanostructures, and alters the morphological integrity.

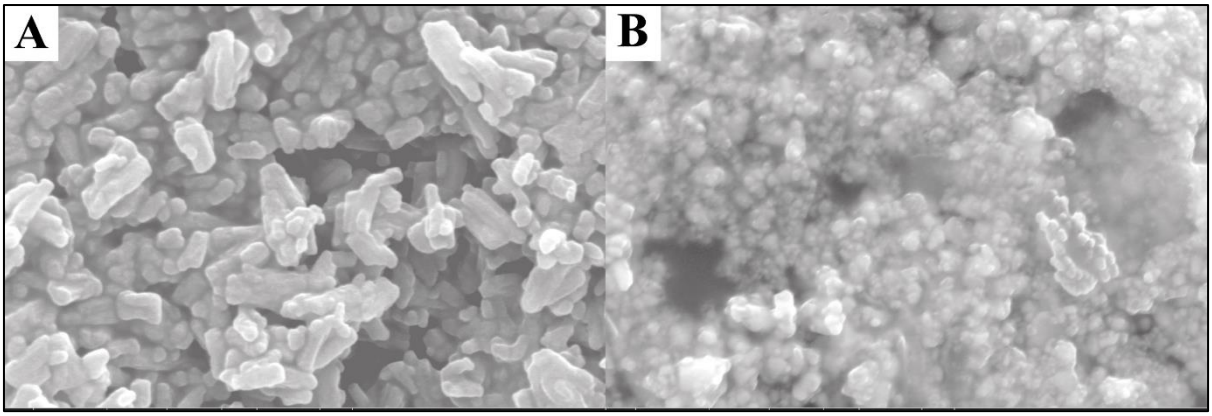

Figure 3 Surface morphology of 5-MESAL-PEI N-GQD (A) and AgNP/5-MESAL-PEI N-GQD (B) as observed by SEM

Elemental compositions were determined through EDS analysis performed on the SEM imaging area of the compound. The EDS results of 5-MESAL-PEI N-GQD, along with the corresponding weight percentages, are presented in Figures 4.

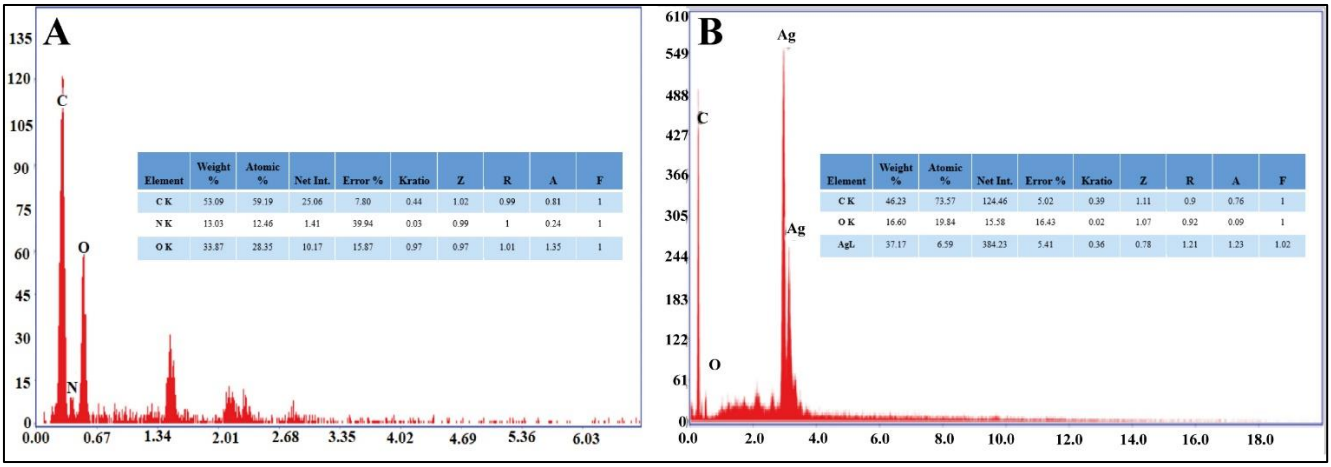

Figure 4 EDS analysis of 5-MESAL-PEI N-GQD (A) and AgNP/5-MESAL-PEI N-GQD (B) showing the elemental distribution

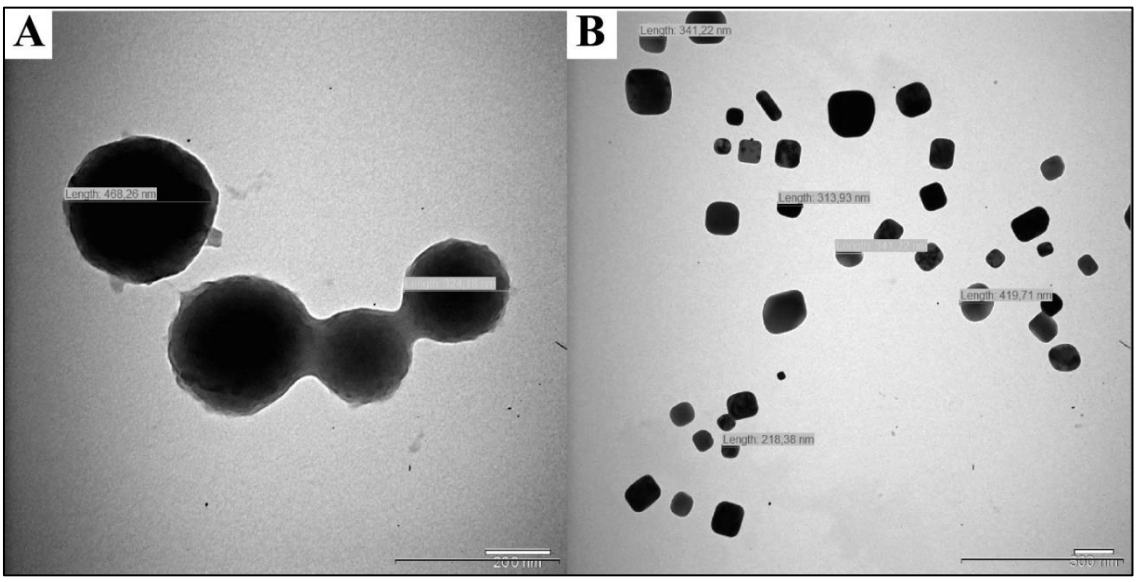

Figure 5 Morphological visualization of 5-MESAL-PEI N-GQD (A) and AgNP/5-MESAL-PEI N-GQD (B) via TEM

TEM characterization was used to further examine the morphology of 5-MESAL-PEI N-GQD and AgNP/5-MESAL-PEI N-GQD Schiff base nanocomposites. The TEM image of the 5-MESAL-PEI N-GQD structures shows that the particles have an irregular, mostly spherical morphology and exhibit pronounced agglomeration behavior, forming large aggregates in the range of approximately 180–460 nm (Figure 5A). The TEM image of the composite structure reveals that the particles in the AgNP/5-MESAL-PEI N-GQD nanostructures have a more defined, uniform, and mostly cuboidal/square geometry (Figure 5B). The particle sizes measured in this image appear to vary between approximately 220–420 nm, suggesting that the silver nanoparticles exhibited a more regular nucleation and growth behavior during composite formation. When the two images are evaluated together, it is understood that the AgNP addition increases the morphological regularity, the particle shape becomes more distinct, and the distribution becomes more homogeneous.

3.2. Biological avtivities of 5-MESAL-PEI N-GQD Schiff Base and AgNP/5-MESAL-PEI N-GQD nanocomposites

3.2.1. DNA binding activities with UV-Vis spectrum

To evaluate the interaction between DNA and the 5-MESAL-PEI N-GQD Schiff base and AgNP/5-MESAL-PEI N-GQD Schiff base nanocomposites, changes in the free absorbance were compared. In the presence of CT-DNA, increasing concentrations of 5-MESAL-PEI N-GQD led to 2-115% hyperchromism and a bathochromic shift (red shift) of approximately 1-3 nm at 258 nm (Figure 6A). Under similar conditions, increasing concentrations of AgNP/5-MESAL-PEI N-GQD resulted in 5-102% hyperchromism and a 1-3 nm bathochromic shift at 269 nm (Figure 6B).

According to the UV-Vis results, both 5-MESAL-PEI N-GQD Schiff base and AgNP/5-MESAL-PEI N-GQD Schiff base nanocomposites were found to interact with CT-DNA through a non-covalent electrostatic binding mode.

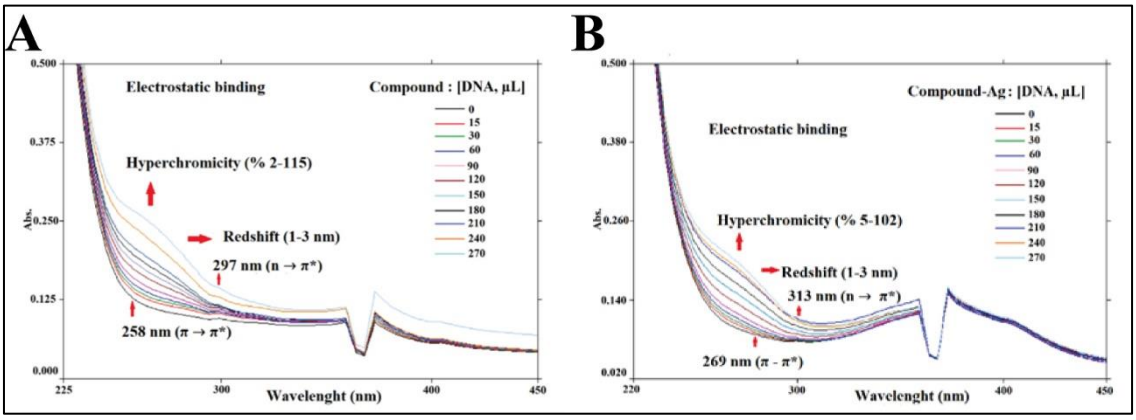

Figure 6 Absorption spectra trace of the 5-MESAL-PEI N-GQD (A) and AgNP/5-MESAL-PEI N-GQD (B) with CT-DNA.

3.2.2. DNA cleavage

The DNA cleavage activities of 5-MESAL-PEI N-GQD and AgNP/5-MESAL-PEI N-GQD were evaluated against pBR322 plasmid DNA at increasing concentrations under both hydrolytic and oxidative conditions.

Both 5-MESAL-PEI N-GQD and AgNP/5-MESAL-PEI N-GQD were found to cleave supercoiled pBR322 plasmid DNA in a concentration-dependent manner, under both hydrolytic (in the absence of any agent) and oxidative conditions (in the presence of H_2O_2 as an oxidizing agent) (Figure 7).

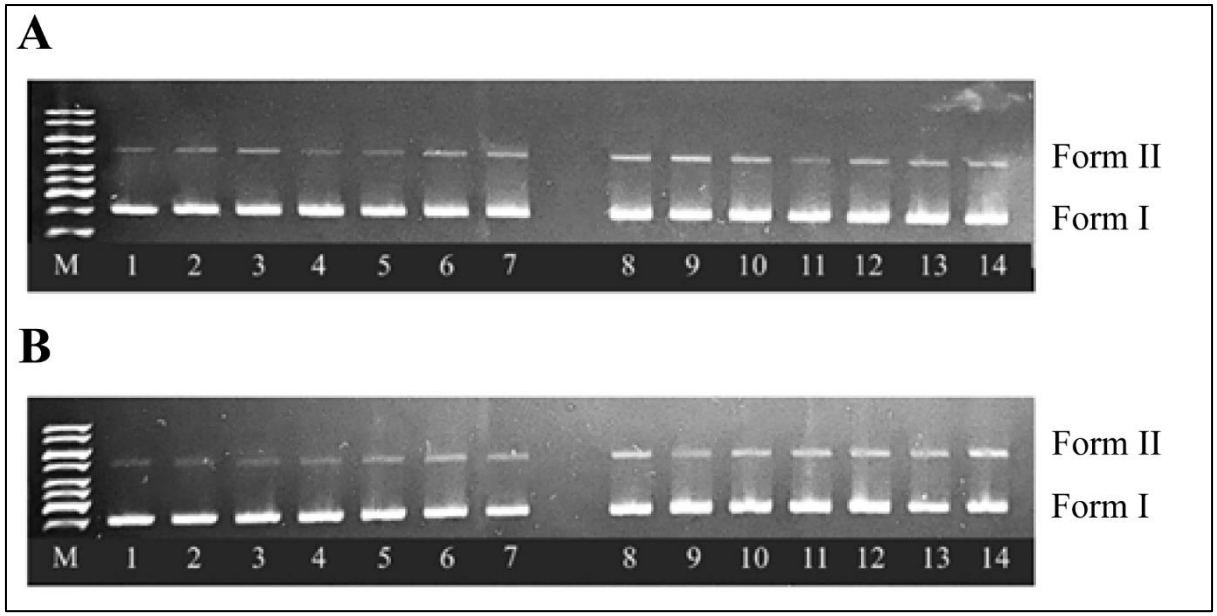

Figure 7 DNA cleavage activities of 5-MESAL-PEI N-GQD (A) and AgNP/5-MESAL-PEI N-GQD (B), 1-7. Hydrolytic DNA cleavage activities, 8-14. Oxidative DNA cleavage activities

1.DNA, 2. DNA + 6.25 ppm, 3. DNA + 12.5 ppm, 4. DNA + 25 ppm, 5. DNA + 50 ppm, 6. DNA + 100 ppm, 7. DNA + 200 ppm, 8. DNA + H_2O_2, 9. DNA + H_2O_2 + 6.25 ppm, 10. DNA + H_2O_2 + 12.5 ppm, 11. DNA + H_2O_2+ 25 ppm, 12. DNA + H_2O_2 + 50 ppm, 13. DNA + H_2O_2 + 100 ppm, 14. DNA + H_2O_2 + 200 ppm.

3.2.3. Antimicrobial activity

The antibacterial and antifungal effects of different concentrations of 5-MESAL-PEI N-GQD and AgNP/5-MESAL-PEI N-GQD on Gram-negative and Gram-positive bacteria as well as yeast species were determined using the minimum inhibitory concentration (MIC) method, which identifies the lowest concentration at which no visible microbial growth is observed. The lowest MIC value for 5-MESAL-PEI N-GQD was observed at 125 ppm against *Proteus vulgaris* and *Enterococcus faecalis*. In contrast, the lowest MIC value for AgNP/5-MESAL-PEI N-GQD was recorded at 3.906 ppm against *Escherichia coli*, *Bacillus subtilis* and *E. faecalis* (Table 1). Compounds exhibiting lower MIC values demonstrate higher antimicrobial activity. When all microorganisms listed in Table 1 are considered, it becomes evident that AgNP/5-MESAL-PEI N-GQD exhibits significantly higher antimicrobial activity compared to 5-MESAL-PEI N-GQD.

Table 1 MIC values (ppm) of the 5-MESAL-PEI N-GQD and AgNP/5-MESAL-PEI N-GQD.

Microorganisms			**5-MESAL-PEI N-GQD (ppm)**	**AgNP/5-MESAL-PEI N-GQD (ppm)**	**Control**	
					Ampicillin	Fluconazole
Bacteria	Gr (-)	*P. vulgaris* (NRRL-B-123)	125	7.813	0.06	-
		P. aeruginosa (ATCC 27853)	500	7.813	2	-
		E. coli (ATCC-25922)	500	3.906	32	-
	Gr (+)	*S. aureus* (ATCC 25923)	500	7.813	0.016	-
		B. subtilis (ATCC 6633)	500	3.906	0.06	-

		E .faecalis (ATCC 29212)	125	3.906	0.016	-
Yeast		*C. albicans* (ATCC 10231)	250	7.813	-	0.063
		C. tropicalis (ATCC 1021)	250	7.813	-	0.5

3.2.4. Antibiofilm activity

Biofilm inhibition values corresponding to the MIC concentrations were also evaluated against various Gram-negative and Gram-positive bacterial strains, as well as yeast strains. The highest biofilm inhibition was observed against *B. subtilis* at 81%, followed by *P. aeruginosa* at 70%. According to the percentage inhibition values illustrated in the graph, 5-MESAL-PEI N-GQD exhibited stronger antibiofilm activity compared to AgNP/5-MESAL-PEI N-GQD (Figure 8).

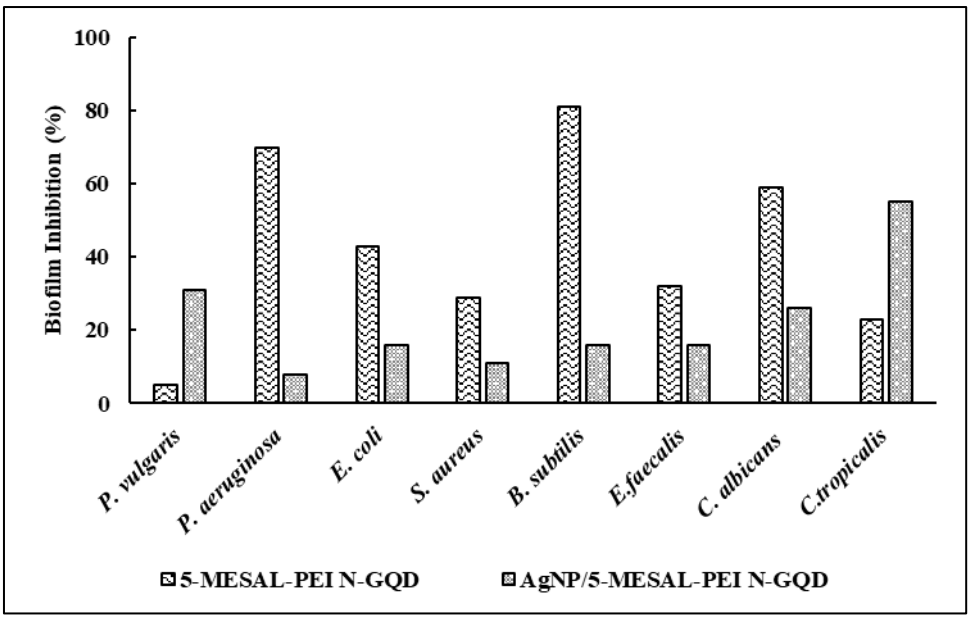

Figure 8 Antibiofilm Activity of 5-MESAL-PEI N-GQD and AgNP/5-MESAL-PEI N-GQD

3.2.5. In vitro antioxidant activity

The antioxidant activities of 5-MESAL-PEI N-GQD and AgNP/5-MESAL-PEI N-GQD at different concentrations (12.5, 25, 50, 100, and 200 ppm) were evaluated using three different assays: DPPH, ABTS, and FRAP. BHT was used as the standard antioxidant in all experiments. Measurements were performed at the characteristic wavelengths of each method, and the percentage of inhibition or increase in absorbance was calculated based on the recorded absorbance values. Overall, in all three methods, the AgNP/5-MESAL-PEI N-GQD nanocomposite exhibited higher antioxidant activity compared to 5-MESAL-PEI N-GQD.

DPPH radical scavenging activity

The DPPH free radical scavenging activity was measured at 517 nm, and the percentage of inhibition was calculated. At the highest concentration of 200 ppm, AgNP/5-MESAL-PEI N-GQD exhibited a higher antioxidant activity with 53.23% inhibition, compared to 5-MESAL-PEI N-GQD, which showed 48.87% inhibition (Figure 9). Overall, the results indicated that the antioxidant efficiency followed the order: AgNP/5-MESAL-PEI N-GQD > 5-MESAL-PEI N-GQD.

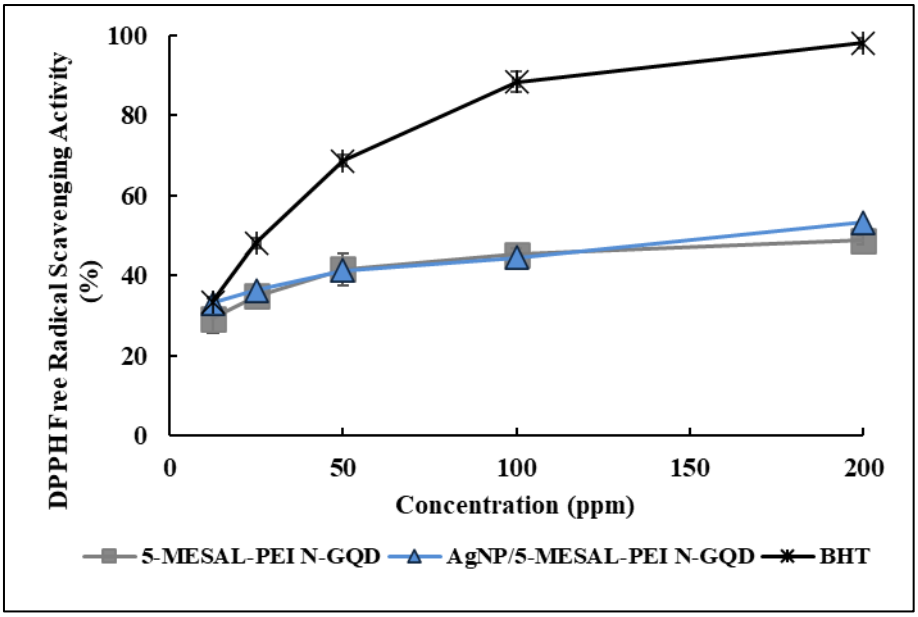

Figure 9 DPPH free-radical scavenging activity of 5-MESAL-PEI N-GQD and AgNP/5-MESAL-PEI N-GQD

ABTS cation radical scavenging activity

The antioxidant activity using the ABTS method was measured at 734 nm inhibition values were calculated. At 200 ppm, AgNP/5-MESAL-PEI N-GQD demonstrated stronger activity with 74.02% inhibition, compared to 5-MESAL-PEI N-GQD, which exhibited 69.59% inhibition (Figure 10). According to the obtained data, both compounds demonstrated high antioxidant capacities, consistently following the trend: AgNP/5-MESAL-PEI N-GQD > 5-MESAL-PEI N-GQD being maintained.

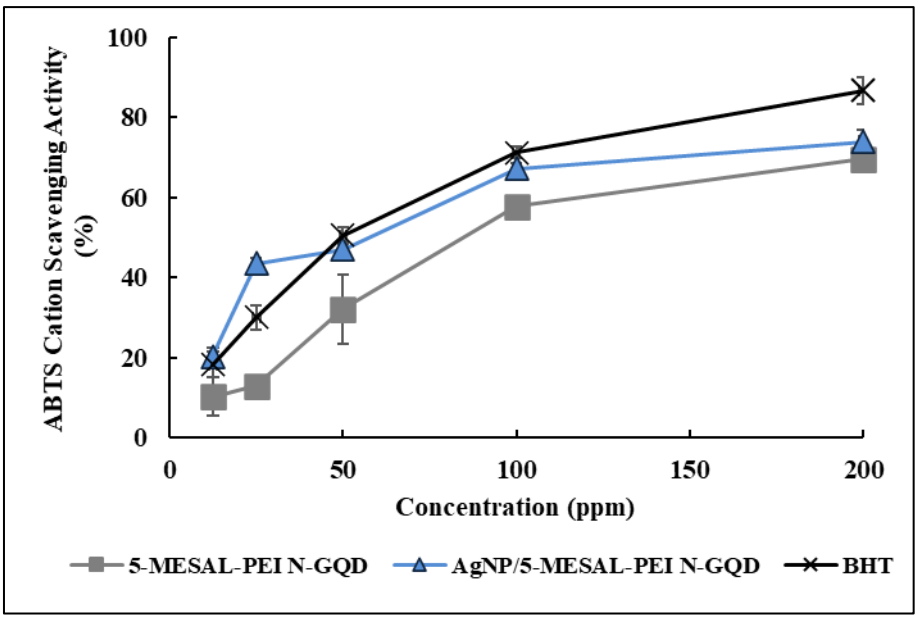

Figure 10 ABTS cation scavenging activity of 5-MESAL-PEI N-GQD and AgNP/5-MESAL-PEI N-GQD

FRAP assay

At a concentration of 200 ppm, AgNP/5-MESAL-PEI N-GQD exhibited a higher antioxidant capacity with an absorbance of 0.864, whereas 5-MESAL-PEI N-GQD demonstrated an absorbance of 0.390 (Figure 11). Additionally, absorbance values increased with increasing concentration for both compounds, indicating a concentration-dependent antioxidant effect.

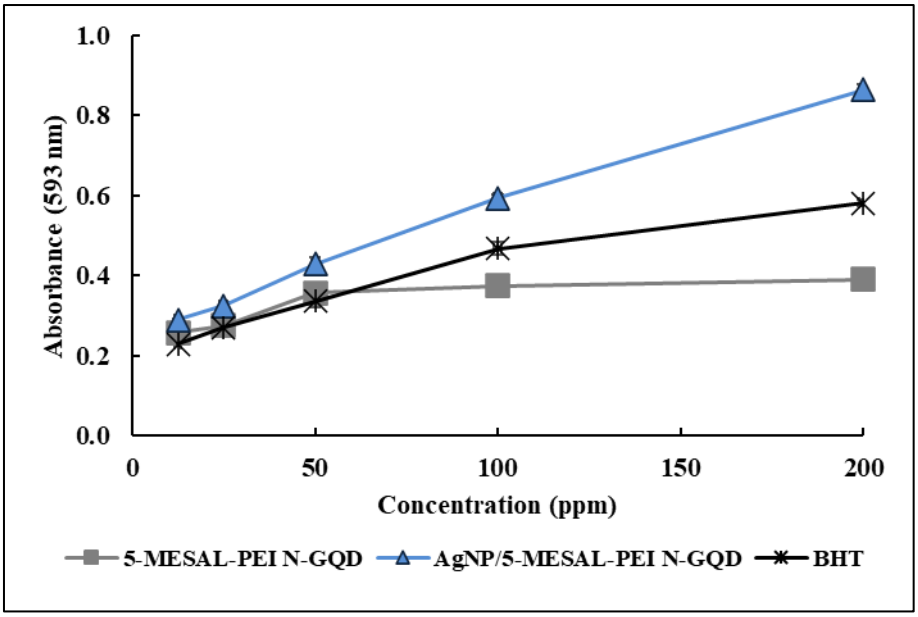

Figure 11 Ferric Reducing Antioxidant Power assay of 5-MESAL-PEI N-GQD and AgNP/5-MESAL-PEI N-GQD

In recent years, nitrogen-doped graphene quantum dots (N-GQDs) and their derivatives have attracted significant attention due to their potential in various biological applications. These nanomaterials, with their diverse biological activities, show great promise as bioactive agents in both biotechnological and clinical fields [30]. In this study, biological activities of 5-MESAL-PEI N-GQDs and AgNP-enhanced hybrid nanocomposites were examined. The results, when compared with similar studies in the literature, demonstrate the multifunctional biological potential of these materials. The synthesis and characterization of the Schiff base and silver (Ag) nanocomposite used in the study are consistent with previous findings [14]. SEM, TEM, and EDS analyses clearly revealed morphological and elemental differences between 5-MESAL-PEI N-GQD and their AgNP-incorporated nanocomposite. The addition of AgNPs resulted in smaller, more homogeneous, and predominantly cubic particles with reduced agglomeration. SEM images confirmed a uniform surface distribution of the particles, while EDS analysis showed carbon as the dominant element, with successful incorporation of oxygen and nitrogen. These findings are consistent with literature reports indicating that AgNP incorporation enhances the structural integrity and stability of GQD-based materials [31-33].

The interaction of graphene quantum dots with DNA has been extensively studied, particularly through gel electrophoresis tests involving pBR322 plasmid DNA, where the conversion of supercoiled to open form is analyzed. Kumawat et al. [34] demonstrated the specific binding of N-GQDs to DNA and their ability to localize within cells, highlighting their potential for nuclear imaging and gene delivery applications. Similarly, Liu et al. [35] reported that N-GQD-based structures form strong electrostatic complexes with plasmid DNA and exhibit low toxicity. The findings of this study also support these observations, as the synthesized 5-MESAL-PEI N-GQDs and their AgNP-enhanced counterparts displayed DNA-binding capability and induced hydrolytic/oxidative cleavage [34, 35].

Silver nanoparticle-enriched carbon-based nanostructures have been intensively studied for their antibacterial and antibiofilm properties. Makky et al. [36] showed that silver nanoparticles, when combined with bacteriophages, can inhibit biofilm formation, while Kubheka et al. [37] reported that graphene-based nanocomposites are effective in both phenanthrene removal and bacterial adsorption. The hybrid composites evaluated in this study also exhibit broad-spectrum antimicrobial activity against both Gram-positive and Gram-negative bacteria, and achieving over 70% inhibition in antibiofilm assays. These results show strong parallels with literature [36, 37]. The antibiofilm and antibacterial activities of AgNP and N-GQD-based hybrid systems suggest their strong potential for use as bioactive agents in clinical applications.

Antioxidant activities, particularly the ability to scavenge reactive oxygen species (ROS), is biologically significant. Zhao et al. [21] reported that graphene-based nanoagents exhibit high scavenging activity in DPPH and ABTS assays. In this study, the AgNP/5-MESAL-PEI N-GQD structure demonstrated approximately 80% scavenging activity in the DPPH assay and values comparable to BHT in the FRAP assay. These results highlight the biological relevance of these nanocomposites in maintaining redox balance [21].

4. Conclusion

Nitrogen-doped graphene quantum dots modified with imino functional groups (5-MESAL-PEI N-GQD) and their silver doped nanocomposite (AgNP/5-MESAL-PEI N-GQD) were successfully synthesized and comprehensively evaluated for their biological activities. UV-Vis analyses conducted with CT-DNA revealed that both nanostructures interact with DNA through a non-covalent, electrostatic binding mode, supported by bathochromic shifts and hyperchromic effects observed in the absorption spectra. Electron-donating ($-NH_2$, -OH) and electron-withdrawing ($-NO_2$) surface groups were found to modulate the DNA binding affinity of GQDs, while AgNP incorporation enhanced the surface charge and increased the number of binding sites, thereby strengthening the interaction with DNA. Furthermore, studies using pBR322 plasmid DNA demonstrated that both structures can induce DNA cleavage under hydrolytic and oxidative conditions. In antimicrobial and antibiofilm assays, AgNP-containing nanocomposites exhibited significant inhibitory activity against Gram-positive and Gram-negative bacteria as well as yeast strains. Antioxidant analyses using DPPH, ABTS, and FRAP assays showed that both structures possessed strong, concentration-dependent free radical scavenging activity, with the Ag-doped variants exhibiting enhanced effects. Collectively, these findings indicate that functionalized N-GQDs and their Ag-based nanocomposites are multifunctional and biocompatible candidates for biomedical applications, while emphasizing the need for further in vivo studies to clarify their pharmacokinetic properties, biocompatibility, and therapeutic potential.

Compliance with ethical standards

Acknowledgments

This research was part of Elif ÜNALDI's Doctorate Thesis Project which was supported by Çanakkale Onsekiz Mart University, The Scientific Research Coordination Unit, Project number: FDK-2023-4395.

The authors thank Çanakkale Onsekiz Mart University, Science and Technology Application and Research Center (ÇOBİLTUM) for characterization.

We also thank Prof. Dr. Mustafa YILDIZ (Department of Chemistry, Faculty of Science, Çanakkale Onsekiz Mart University) for the synthesis of compounds used in this study.

Disclosure of conflict of interest

No conflict of interest to be disclosed.

References

[1] Novoselov KS, Geim AK, Morozov SV, Jiang D, Zhang Y, Dubonos SV, Grigorieva IV, Firsov AA. Electric field effect in atomically thin carbon films. Science. 2004; 306(5696): 666-69.

[2] Pramanik K, Saren S, Mitra S, Ghosh PK, Maiti TK. Computational elucidation of phylogenetic, structural and functional characteristics of Pseudomonas Lipases. Computational Biology and Chemistry. 2018; 74: 190-200.

[3] Chung C, Kim YK, Shin D, Ryoo SR, Hong BH, Min DH. Biomedical applications of graphene and graphene oxide. Accounts of Chemical Research. 2013; 46(10): 2211-24.

[4] Peng B, Shen Y, Li X, Chen X, Hou J, Bao X. Improvement of xylose fermentation in respiratory-deficient xylose-fermenting *Saccharomyces cerevisiae*. Metabolic Engineering. 2012; 14 (1):9-18.

[5] Singh P, Shandilya P, Raizada P, Sudhaik A, Rahmani-Sani A, Hosseini-Bandegharaei A. Review on various strategies for enhancing photocatalytic activity of graphene based nanocomposites for water purification. Arabian Journal Chemistry. 2020; 13(1): 3498-520.

[6] Ahmad SZN, Wan Salleh WN, Ismail AF, Yusof N, Mohd Yusop MZ, Aziz F. Adsorptive removal of heavy metal ions using graphene-based nanomaterials: Toxicity, roles of functional groups and mechanisms. Chemosphere. 2020; 248: 126008.

[7] Xia MY, Xie Y, Yu CH, Chen GY, Li YH, Zhang T, Peng Q. Graphene-based nanomaterials: the promising active agents for antibiotics-independent antibacterial applications. Journal of Controlled Release. 2019; 307: 16-31.

[8] Baig N, Ihsanullah, Sajid M, Saleh TA. Graphene-based adsorbents for the removal of toxic organic pollutants: A review. Journal of Environmental Management. 2019; 244:370-382.

[9] Tan B, Thomas NL. A review of the water barrier properties of polymer/clay and polymer/graphene nanocomposites. Journal of Membrane Science. 2016;514:595-612.

[10] Ahn M, Song J, Hong BH. Facile synthesis of N-doped graphene quantum dots as novel transfection agents for mRNA and pDNA. Nanomaterials. 2021; 11(11): 2816.

[11] El-Nour KMMA, Eftaiha A, Al-Warthan A, Ammar RAA. Synthesis and applications of silver nanoparticles. Arabian Journal of Chemistry. 2010;3(3): 135-140.

[12] Mittal AK, Chisti Y, Banerjee UC. Synthesis of metallic nanoparticles using plant extracts. Biotechnology Advances. 2013; 31(2): 346-356.

[13] Ouled Ltaief O, Ben Amor I, Hemmami H, Hamza W, Zeghoud S, Ben Amor A, Benzina M, Alnazza Alhamad A. Recent developments in cancer diagnosis and treatment using nanotechnology. Annals of Medicine and Surgery. 2024; 17,86(8): 4541-4554.

[14] Hançe S, Erdener D, Öztürk BI, Akhüuseyin Yıldız E, Karatay A, Boyacıoğlu B, Ünver H, Yılmazer A, Yıldız M, Elmalı A. Exploring Charge Transfer Mechanisms in Schiff Base-Modified N-Doped GQDs: Insights from DFT and Pump-Probe Spectroscopy for Bioimaging Applications. Chemistry Select. 2024; 9(41): e202403920.

[15] Li C, Guo L, Zang B, Lu L. Graphene quantum dots mediated electron transfer in DNA base pairs. RSC Advances. 2019; 9: 31636-31644.

[16] Lu H, Li W, Dong H, Wei M. Graphene quantum dots for optical bioimaging. Small. 2019;15(36): 1902136.

[17] Liang G, Shi H, Qi Y, Li J, Jing A, Liu Q, Feng W, Li G, Gao S. Specific Anti-biofilm Activity of Carbon Quantum Dots by Destroying *P. gingivalis* Biofilm Related Genes. International Journal of Nanomedicine. 2020; 15: 5473-89.

[18] Henna TK, Pramod K. Graphene quantum dots redefine nanobiomedicine. Materials Science and Engineering: C. 2020; 110:110651. https://doi.org/10.1016/j.msec.2020.110651

[19] Ajiboye TO, Komolafe YO, Oloyede OB, Ogunbode SM, Adeoye MD, Abdulsalami IO, Nurudeen QO. Polyphenolic extract of *Sorghum bicolor* grains enhances reactive oxygen species detoxification in N-nitrosodiethylamine-treated rats. Food Science and Human Wellness. 2013;2(1):39-45.

[20] Choudhary P, Biswas S, Kandoth N, Tayde D, Chatterjee A, Chattopadhyay S, Das A, Swarnakar S, Pramanik SK. Graphene quantum dots alleviate ROS-mediated gastric damage. iScience. 2022;25(4):105062.

[21] Zhao L, Wang Y, Li Y. Antioxidant Activity of Graphene Quantum Dots Prepared in Different Electrolyte Environments. Nanomaterials. 2019;9(12):1708.

[22] Facure MHM, André RS, Mercante LA, Correa DS. Colorimetric Detection of Antioxidants in Food Samples Using MnO_2/Graphene Quantum Dot Composites with Oxidase-like Activity. ACS Applied Nano Materials. 2022; 5 (10): 15211-15219.

[23] Qiao X, Ma ZY, Xie CZ, Xue F, Zhang YW, Xu JY, Qiang ZY, Lou JS, Chen GJ, Yang SP. Study on Potential Antitumor Mechanism of a Novel Schiff Base Copper (II) Complex: Synthesis, Crystal Structure, DNA Binding, Cytotoxicity and Apoptosis Induction Activity. Journal of Inorganic Biochemistry. 2011;105 (5):728-737.

[24] CLSI. Clinical and Laboratory Standarts Institute. Methods for Dilution Antimicrobial Susceptibility Tests for Bacteria That Grow Aerobically. Approved Standard-7th ed.; CLSI document M07- A7. Villanova, PA, USA; 2006.

[25] Issenberg HD. Essential Procedures for Clinical Microbiology. American Society for Clinical Microbiology, Washingtoon DC. 1998;126-223.

[26] Merritt JH, Kadouri DE, O'Toole GA. Growing and analyzing static biofilms. Current Protocols in Microbiology. 2005; 1: 1B.1.1-1B.1.18.

[27] Blois MS. Antioxidant determinations by the use of a free free radical. Nature. 1958;181: 1199- 200.

[28] Re R, Pellegrini N, Proteggente A, Pannala A, Yang M, Rice-Evans C. Antioxidant activity applying an improved ABTS radical cation decolorization assay. Free Radical Biology and Medicine. 1999;26(9-10):1231-1237.

[29] Benzie IFF, Strain JJ. The ferric reducing ability of plasma (FRAP) as a measure of "antioxidant power": The FRAP assay. Analytical Biochemistry. 1996;239(1):70-76.

[30] Le N, Kim K. Current Advances in the Biomedical Applications of Quantum Dots: Promises and Challenges. International Journal of Molecular Sciences. 2023;24(16):12682.

[31] Habiba K, Bracho-Rincon DP, Gonzalez-Feliciano JA, Villalobos-Santos JC, Makarov VI, Ortiz D, Avalos JA, Gonzalez CI, Weiner BR, Morell G. Synergistic antibacterial activity of PEGylated silver–graphene quantum dots nanocomposites. Applied Materials Today. 2015;1(2):80-87.

[32] Sun H, Wu L, Wei W, Qu X. Recent advances in graphene quantum dots for sensing. Materials Today. 2013;16(11): 433-442.

[33] Zhao C, Song X, Liu Y, Fu Y, Ye L, Wang N, Wang F, Li L, Mohammadniaei M, Zhang M, Zhang Q, Liu J. Synthesis of graphene quantum dots and their applications in drug delivery. Journal of Nanobiotechnology. 2020;18(142):1477-3155.

[34] Kumawat MK, Thakur M, Gurung RB, Srivastava R. Graphene quantum dots for cell proliferation, nucleus imaging, and photoluminescent sensing applications. Scientific Reports. 2017;7(1):15858.

[35] Liu H, Yang Z, Xun Z, Gao Z, San Y, Yu J, Xiaoyun Z, Cai C, Ding P. Nuclear delivery of plasmid DNA determines the efficiency of gene expression. Cell Biology International. 2019;43(7): 789-798.

[36] Makky S, Rezk N, Abdelsattar AS, Hussein AH, Eid A, Essam K, Kamel A, Fayez MS, Azzam M, Agwa MM, El-Shibiny A. Characterization of the biosynthesized *Syzygium aromaticum*-mediated silver nanoparticles and its antibacterial and antibiofilm activity in combination with bacteriophage. Results in Chemistry. 2023; 100686.

[37] Kubheka G, Adeola AO, Ngulube R, Nombona N, Forbes PBC. Magnetic hexadecylamine-graphene quantum dots-silver nanoparticle nanocomposite as adsorbents for the removal of phenanthrene and bacteria from aqueous solution. Discover Applied Sciences. 2024; 6:474.